Since January 2020 Elsevier has created a COVID-19 resource centre with free information in English and Mandarin on the novel coronavirus COVID-19. The COVID-19 resource centre is hosted on Elsevier Connect, the company's public news and information website.

Building and Environment 77 (2014) 119–134

Contents lists available at ScienceDirect

Building and Environment

journal homepage: www.elsevier.com/locate/buildenv

The influence of human walking on the flow and airborne transmission in a six-bed isolation room: Tracer gas simulation

Jian Hang [a], Yuguo Li [b,*], Ruiqiu Jin [a]

[a] Department of Atmospheric Sciences, School of Environmental Science and Engineering, Sun Yat-Sen University, Guangzhou, PR China
[b] Department of Mechanical Engineering, The University of Hong Kong, Haking Wong Building, Pokfulam Road, Hong Kong Special Administrative Region

ARTICLE INFO

Article history:
Received 4 February 2014
Received in revised form
27 March 2014
Accepted 29 March 2014
Available online 12 April 2014

Keywords:
Isolation room
Ventilation
Human walking
Computational fluid dynamic (CFD) simulation
Airborne transmission

ABSTRACT

By performing unsteady CFD simulations using RNG $k-\varepsilon$ model and dynamic mesh technique, this paper investigates how the walking motion of health care worker (HCW) influences gaseous dispersion in a six-bed isolation room with nine downward supplies and six ceiling-level or floor-level exhausts. The flow near and behind HCW is easily affected by HCW motion. The flow disturbance induced by HCW walking with swinging arms and legs is a mixing process. The walking HCW displaces air in front of it and carries air in the wake forwardly, meanwhile pressure difference drives air from two lateral sides into the wake. HCW motion (0–5.4 s) indeed induces a little gaseous dispersion, but the residual flow disturbance after HCW stops (5.4 s–25.4 s) induces more gaseous agent spread and it requires more than 30–60 s to approximately recover to the initial state after HCW stops.

Although HCW motion indeed affects airborne transmission, but its effect is less important than ventilation design. No matter with or without HCW motion, the ceiling-level exhausts perform much better in controlling airborne transmission than the floor-level exhausts with the same air change rate (12.9 ACH). Smaller air change rate of 6 ACH experiences higher concentration and more gaseous spread than 12.9 ACH. In contrast to the realistic human walking, the simplified motion of a rectangular block produces stronger flow disturbance. Finally surface heating of HCW produces a stronger thermal body plume and enhances turbulence near HCW, thus slightly strengthens airborne transmission.

1. Introduction

Airborne transmission is one of the main spread routes for a number of infectious diseases including smallpox, tuberculosis, severe acute respiratory syndrome (SARS) and influenza [1–5]. Specially there is an expected high risk of infection from patients to health care workers (HCWs) and other patients during an outbreak of such airborne diseases in hospitals [2–5]. The aim of mechanical ventilation systems with supplies and exhausts is to control air movements to protect HCWs and other patients from the polluted air by the infected patients. Effective mechanical ventilation design has been considered to be important for minimizing transmission of airborne diseases in hospital isolation rooms [2–5].

There have been a number of related full-scale experiments and computational fluid dynamic (CFD) simulations studying how different ventilation systems disperse and remove gaseous contaminants, exhaled particles and droplets from various indoor environments [1–20]. The displacement ventilation has been considered effective and widely used for indoor air quality control in general indoor environments [20], however in hospital isolation rooms, Qian et al. [14] and Yin et al. [19] found that the displacement ventilation may or may not provide a better performance of removing tracer gas and/or fine particles in the breathing zone depending on the location of the exhaust. Previous investigations on mixing ventilations in hospital isolation rooms [17,18] suggested that, if the upward thermal body plumes are considered in an isolation room with downward supply air streams, the ceiling-level exhausts are more efficient than the floor-level exhausts in reducing airborne transmissions. Some literature [3,21,22] provided good reviews.

In recent years, a few investigations have indicated that transient events such as human movements play an important role on indoor dynamic airflows and contaminant dispersion [23–34]. However full-scale experimental investigations of how human movements affect dynamic airflows and airborne transmission are difficult and high-quality experimental data with meaningful temporal and spatial resolution are rare so far [23–27]. The application of dynamic mesh technique combined with CFD simulations

* Corresponding author. Tel.: +86 852 28592625; fax: +86 852 2858 5415.
E-mail addresses: hangj3@mail.sysu.edu.cn (J. Hang), liyg@hku.hk (Y. Li).

http://dx.doi.org/10.1016/j.buildenv.2014.03.029
0360-1323/

provides a promising tool for such investigations [26–34]. Poussou et al. [27] and Mazumdar et al. [28] carried out small-scale experiments and CFD simulations to study the impact of human movement on airborne transmission in airliner cabins, finding that the human-induced wake may carry contaminant to positions far from the source location. Choi and Edward [29,30] performed large eddy simulations to explore how realistic human walking affects indoor airflows and contaminant transport between two rooms through a door way and the shared hall or vestibule. They first found that [29] the human wake may transport material over a distance of 8 m when there is no ventilation system. The walking speed and the initial proximity of human from the doorway may affect the human-induced room-to-room contaminant transport. Then they reported that [30], with ventilation systems, human-induced wake motion did enhance compartment-to-compartment contaminant transport.

Reported nosocomial SARS outbreaks in hospital wards worldwide have reminded us that it requires to create a safe and healthy environment in hospital wards, i.e. protect HCWs and uninfected patients from the risk of infection during an outbreak of airborne or droplet-borne diseases. In hospital isolation rooms, there are usually mechanical ventilation systems with air change rates of higher than 4–6 ACH, which are higher than general mechanically-ventilated indoor environments. Thus the effect of HCW motion on dynamic airflow and airborne transmission in hospital isolation rooms possibly differs from other kinds of rooms and requires more special concern. Previous studies usually used a sharp-edged rectangular block to model a moving HCW in an one-bed isolation room [31–33]. The use of rectangular blocks possibly over-predicts the dynamic flow disturbance induced by HCW motion, considering that a realistic walking HCW is a moving blunt object with human profile [35] and swinging legs, moreover there is leakage between torso and arms as well as between two legs [29,30]. Shih et al. [31] found that although the velocity and pressure fields in an one-bed isolation room are easily affected by a moving person, however the moving body does not obviously affect the removal of gaseous contaminants. Mazumdar et al. [32] verified that the wake of moving objects can carry gaseous contaminants inducing a swing in the contaminant concentration at the breathing levels for 10–90 s, but the risk level in the ward change little with and without the movements. Wang and Chow [33] numerically investigated the effect of human walking on dispersion and deposition of expiratory particles (0.5–20 μm) in an one-bed isolation room, finding that HCW motion significantly affects the particles dispersion and depositions. The faster HCW motion, the less suspended particles in the isolation room. The findings of Wang and Chow [33] differ from the other two [31,32]. The possible reason is that, in Wang and Chow [33], the boundary conditions at all wall surfaces (i.e. including moving object) for particles is 'trap' condition with 'deposition effect', and particles may deposit onto HCW surfaces as it moves backwards and forwards, however for gaseous contaminants there is no deposition [31,32]. In addition, some literature treated the patient as the only heat source [31,33], and some considered the heat flux from HCW surface [32]. Further investigations are still required to investigate the difference between these two situations. Finally, apart from human movement, the influence of other transient events in enclosed indoor environments has also been investigated, such as changing of sheets on a patient's bed [32], the motion of door opening and closing [4,29–31,36–38].

The purpose of this paper is to investigate how human walking influences the flow and airborne transmission in a six-bed hospital ward [18] which consists of different ventilation systems with nine downward supplies and either ceiling-level or floor-level exhausts. Respiratory material includes gaseous contaminants, exhaled particles and droplets. As a start, this paper only considers gaseous contaminants released from the source manikin's mouth. The following questions will be explored.

(1) What are the aerodynamic effects of a nearly realistic HCW walking and how it affects airborne transmission in a six-bed hospital isolation room?
(2) As verified by Qian and Li [18], the ceiling-level exhausts are confirmed more effectively in controlling airborne transmission than the floor-level exhausts. Is there the same conclusion when HCW walking occurs?
(3) For the ceiling-level exhausts with HCW walking, what changes for airborne transmission by lowering air change rate from 12.9 to 6 ACH?
(4) Is there difference when the realistic HCW walking is replaced by a simplified motion of a rectangular block? What difference occurs if the surface heat flux of HCW model is taken into account?

2. Methodologies

2.1. Modelling realistic human walking

Ronan et al. [39] studied the walking characteristics of human body. As shown in Fig. 1a (revised from the figure in Ronan et al. [39]), the swinging motion of both legs and arms is controlled by a temporal profile. If the normalized walking cycle events are mapped on the interval [0, 1] and the associated phase variable ϕ denotes the progression in the cycle, almost all the walking cycle events have a constant phase value whatever the walking velocity is [39]. Here $\phi = ft = t/T$ (f is the walking frequency, T is the cycle duration (s)). For the total hip flexion amplitude Δhip (see Fig. 1a), Ronan et al. [39] suggested a choice of $\text{hip}_{\max} = -2\ \text{hip}_{\min}$ which is

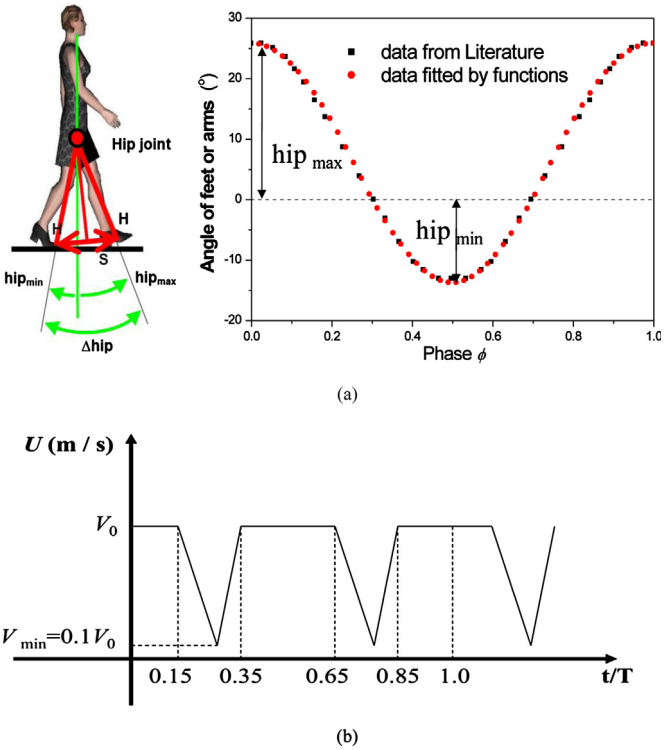

Fig. 1. Walking control and pattern according to Ronan et al. (2004): (a) Angle of feet and arms as human walking, (b) Moving velocity of human body (U, m/s).

consistent with values observed in the natural walking pattern. Here in our CFD simulations (see Figs. 1a and 2b), $H = 0.68$ m is the leg length for the walking HCW model. Moreover, as shown in Fig. 1b, the acceleration or deceleration of moving speed is linear as a function of ϕ or time t (s) during human walking. We also assume that a HCW would walk softly with an average speed of 0.89 m/s (or 2 mph) according to the classification of Ainsworth et al. [40], and the key parameters include the frequency $f = 0.74$ Hz (or $T = 1.35$ s), the total hip flexion amplitude Δhip $= 38.9°$, the maximum walking velocity $V_0 = 1.09$ m/s and the minimum walking velocity $V_{min} = 0.11$ m/s. The arms can be swinging or not swinging depending on the activity pattern (for example, carrying something using two hands). Here we assume that arms also swing in the opposite phase of legs (i.e. the left arm swings similarly to the right leg).

2.2. CFD setups for flow modelling and dynamic mesh

Indoor airflows are generally turbulent, which can be simulated by LES (Large Eddy Simulation) and RANS (Reynolds Averaged Navier–Stokes) turbulence models. The applications of LES to CFD simulations of unsteady flow fields with human movement require very demanding computer memory and a long calculation time [29,30].

For the RANS turbulence models, Zhang et al. [44,45] reported that the RNG k–ε model [42] was one of the best turbulence models in terms of accuracy, computing efficiency, and robustness for modelling indoor environments in comparison to other RANS approaches. Thus RNG k–ε model was adopted in this study.

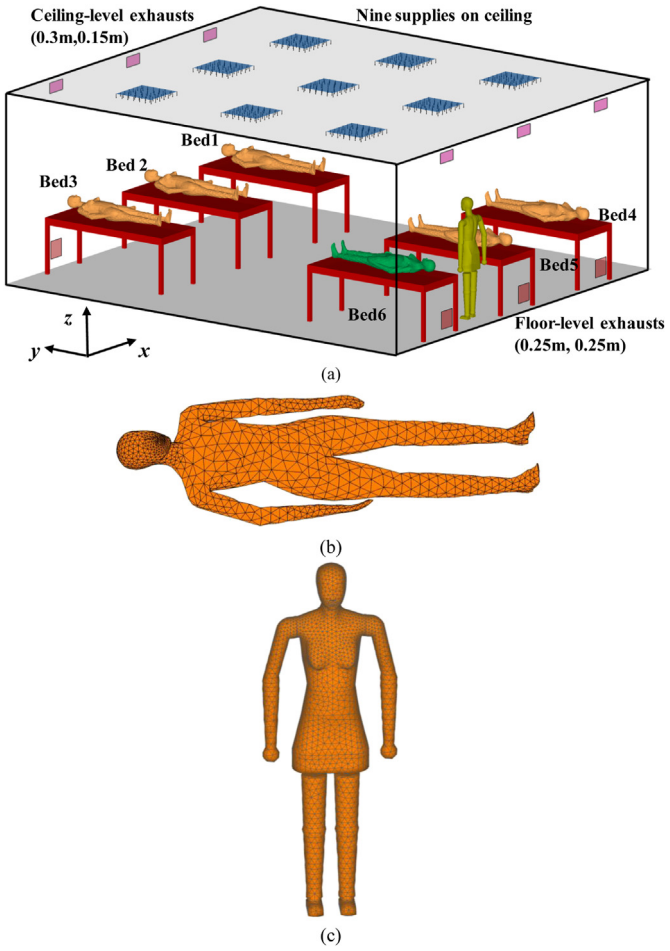

Fig. 2. Model setups in present CFD simulations: (a) the six-bed isolation room, (b) the lying patient, (c) the standing HCW model (Blunt body A).

The CFD software FLUENT 6.3 [41] was utilized to simulate the indoor turbulent flow and the aerodynamic effects of human movement. The Boussinesq model was employed for the buoyancy effect. The integral form of the conservation equation for a general scalar, on an arbitrary control volume *Vol* with moving boundary can be written as [41]:

$$\frac{\mathrm{d}}{\mathrm{d}t}\int_{\mathrm{Vol}}\rho\phi\,\mathrm{d}x\mathrm{d}y\mathrm{d}z+\int_{\partial\mathrm{Vol}}\rho\phi\left(\vec{V}-\vec{V_g}\right)\cdot\mathrm{d}\vec{A}=\int_{\partial\mathrm{Vol}}\Gamma\nabla\phi\cdot\mathrm{d}\vec{A}+\int_{\mathrm{Vol}}S_\phi\,\mathrm{d}x\mathrm{d}y\mathrm{d}z \quad (1)$$

where ρ is the fluid density, $\vec{V}$ is the flow velocity vector, $\vec{V_g}$ is the grid velocity of the moving mesh, Γ is the diffusion coefficient, S_ϕ is the source term, and ∂Vol represents the boundary of the control volume. More details about the discretization of individual terms of governing equations and moving grid can be referred to Fluent [41].

The conservation governing equations were discretized by a finite volume method (FVM). The SIMPLE algorithm was used to decouple pressure and velocity. To improve numerical accuracy, the second-order upwind scheme was used for discretizing the convection and diffusion–convection terms in the governing equation. The simulations were assumed to converge if the residuals for mass, energy, and tracer gas were less than 1.0×10^{-3}, 1.0×10^{-6}, and 1.0×10^{-5} respectively. Each case was computed in a 2-node CPU cluster, and each node had sixteen processors (2.4 GHz Intel 64). The calculation of each case spent about 2–3 weeks depending on the total number of time steps and iterations.

As displayed in Fig. 2, the geometry of the simulated six-bed isolation room was set the same as the full-scale test room in the University of Hong Kong [18]. The room is 6 m long (x), 6.7 m wide (y) and 2.7 m tall (z). There are six thermal manikins lying on Bed 1 to Bed 6 to mimic patients (Patient 1 to Patient 6) at rest. Each bed is 0.8 m wide (x), 2 m long (y) and 0.8 m tall (z). The distance between two neighboring beds at one side is 1 m. All boundary conditions

Table 1
Computational domain, geometry information of objects and boundary conditions used.

Computational domain	6 m long (x), 6.7 m wide (y), 2.7 m tall (z)
Nine downward supplies (0.6 m × 0.6 m)	Supply velocity 0.12 m/s, $T = 293.15$ K, air change rate of 12.9 ACH
Six ceiling-level exhausts (0.3 m × 0.15 m)	Outflow (zero normal gradient) boundary as they are opened; No slip wall boundary as they are closed
Six floor-level exhausts (0.25 m × 0.25 m)	
Thermal manikin of patients (surface area 1.47 m^2)	No slip wall boundary, standard wall function, 26 Watt/m^2
Ceiling and floor	16 Watt/m^2 at ceiling surface and 5.1 Watt/m^2
Body A for nearly realistic walking motion (surface area 1.6 m^2)	With legs and arms, No slip wall boundary, standard wall function, zero heat flux in Case 1 to Case 4 and 57.5 Watt/m^2 in Case 5
Body B (surface area 1.6 m^2)	Simplified sharp-edged rectangular block (1.6 m tall)
Six beds and walls	No slip wall boundary, standard wall function
Mouth of source thermal manikin on Bed 6	Continuous release with an upward exhalation velocity 0.107 m/s, mass fraction of carbon monoxide is 0.04.

and geometries including supplies, exhausts, thermal manikins and wall surfaces are shown in Table 1. Zero normal gradient boundary condition was used at six ceiling-level or floor-level exhausts. No slip boundary conditions with standard wall functions were set at wall surfaces to treat the turbulent flow properties in the near wall regions [41]. The default downward air supply from nine ceiling diffusers provided an air change rate of 12.9 ACH (i.e. the mean flow velocity $U = 0.12$ m/s). Moreover, the turbulence kinetic energy k and its dissipation rate ε employed in the nine supplies were calculated by the following equations:

$$k = 1.5(UI)^2 \tag{2a}$$

$$\varepsilon = C_\mu^{3/4}\left(k^{3/2}/l\right) \tag{2b}$$

$$l = 0.07D_h \tag{2c}$$

where I is the turbulence intensity, D_h is the hydraulic diameter and $C_\mu = 0.09$.

We assumed that half the heat from the lying thermal manikins was transferred through convection [18,46]. Considering the total heat of 76 Watt [46] produced by the manikin and its surface area of 1.47 m^2, the convection heat flux (sensible heat emission) at skin surfaces of lying patients was defined as 26 Watt/m^2. The radiation parts from thermal manikins and light were assumed to be distributed at other wall surfaces. The radiation physical process was not simulated, but the thermal boundary conditions at wall surfaces in this paper following our previous studies (see Table 1) in Qian and Li [18]. The grid size for the surface of lying thermal manikins (see Fig. 2b) is from 0.5 cm to 5 cm for which the finest near mouth, fine near the head and relatively coarse near torso surface. The grid size at HCW surfaces is 2 cm, and the maximum grid size at wall surfaces is 10 cm. The total number of tetrahedral cells is about 0.9 million. This grid arrangements are similar with those in our previous CFD simulations [18] and those in the literature [31,32]. The default air change rate in present investigations is 12.9 ACH, thus the characteristic temporal scale is in order of 5 min. Two situations for thermal boundary conditions at HCW surfaces were considered. One assumes that HCW model only stays near the source manikin (Patient 6) for a short moment (much less than 5 min) and there is no heat flux from the HCW surface. The other supposes that HCW model has been staying there for sufficiently long time (for example ~10 min), and the surface heat flux (57.5 Watt/m^2) of HCW model should be considered.

We first obtained the steady-state solutions for the airflow field, then tracer gas was continuously released into the ward through the source manikin's mouth in Bed 6 at a mass fraction of 0.04 with an upward exhalation velocity of 0.107 m/s. The height of source location (mouth of Patient 6) is 1.06 m. For the transport equation of tracer gas, zero normal gradient boundary condition at exhausts and zero normal flux boundary condition at wall surfaces were used. The initial conditions inside the ward were steady-state with a continuous release. Gupta et al. [47,48] found that the momentum of exhalation was important for coughing but not significant for breathing and talking. Thus, the tracer gas release in this paper could be acceptable.

To investigate the difference of flow disturbance induced by realistic human walking and simplified motion, two kinds of HCW models are included. One is a nearly realistic human body (body A, see Fig. 2c) with a height of 1.7 m and surface area of 1.6 m^2. The motion of body A is controlled as in Fig. 1, including the forwardly moving torso with periodically varying speed and periodic motion of swinging legs and arms. The other is a simple sharp-edged rectangular body (body B, not shown here) which is 1.6 m tall (z), 0.32 m wide (x) with the same total surface area of 1.6 m^2 and without legs and arms. This simple body B only moves forward with the same average speed of 0.89 m/s. In all test cases, the HCW starts to walk at time of 0 s, and walks for 5.4 s to the other side of the isolation room, then stops and stays there for several minutes. During human walking ($t = 0$ s–5.4 s), a user defined function (UDF) was dynamically loaded to realize HCW walking. The average walking speed is 0.89 m/s, thus the total walking distance is about

Table 2
Four test cases investigated.

Case name	Air change rate (ACH)	Ceiling-level exhausts	Floor-level exhausts	Model description of human walking
1	12.9	Open	Close	Body A[a]
2	12.9	Close	Open	Body A
3	6	Open	Close	Body A
4	12.9	Open	Close	Body B[a]
5	12.9	Open	Close	Body A with surface heat flux (57.5 Watt/m^2)

[a] Body A is for realistic blunt body with swinging arms and legs, Body B is a rectangular block with simple motion.

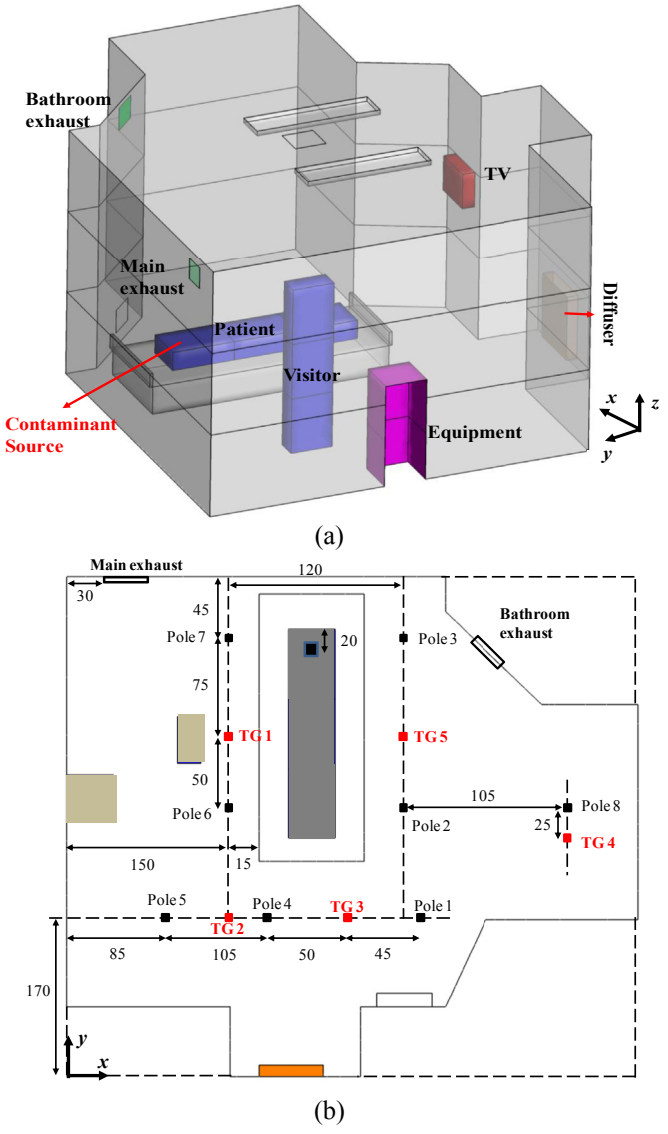

Fig. 3. Model description of the one-bed isolation room in Yin et al. [19].

Table 3
Boundary conditions for the inpatient ward in the validation case.

Supply airflow rate	4 ACH	Heat released from the visitor	110 Watt
Supply air temperature	19.5 °C	Heat released from the patient	106 Watt
Ceiling surface temperature	22.5 °C	Heat released from the equipment	36 Watt
Surface temperature of the side walls	22.5 °C	Heat released from the TV	24 Watt
Floor temperature	22 °C		

4.8 m. The minimum time step for unsteady CFD simulation is 0.02 s.

Overall, selecting a reliable turbulence model, boundary conditions, numerical scheme and numerical algorithm can improve the accuracy of simulating indoor airflows. The CFD approaches adopted are similar with those of Qian and Li [18], Shih et al. [31] and Mazumda et al. [32].

2.3. Test cases investigated

It is worth mentioning that, most airborne transmissions are droplets/particles dispersion. The main difference between tracer gas and particles is that, the gravity force and the deposition effect are important to particle distribution [6–11,18,19,49]. Zhao and Wu [49] found that ventilation mode, particle source location and air exchange rate play important roles on indoor particle diffusions. For particles with sizes of 0.3–20 μm, if the product of nominal time of a ventilated room and the particle relaxation time is big enough, the particle diffusions significantly differ from tracer gas. Qian and Li [18] found that large particles (>20 μm) may rapidly deposit onto wall surfaces, and ventilation modes are key to the removal of fine particles (~0.5–10 μm). Yin et al. [19] experimentally verified the distributions of gaseous contaminant and fine particles (1 and 3 μm) looked the same. Thus ventilation rates and airflow patterns are important to transmit and remove gaseous agents and exhaled fine particles. In addition, a long period of human walking forwards and backwards [31–33] possibly produce

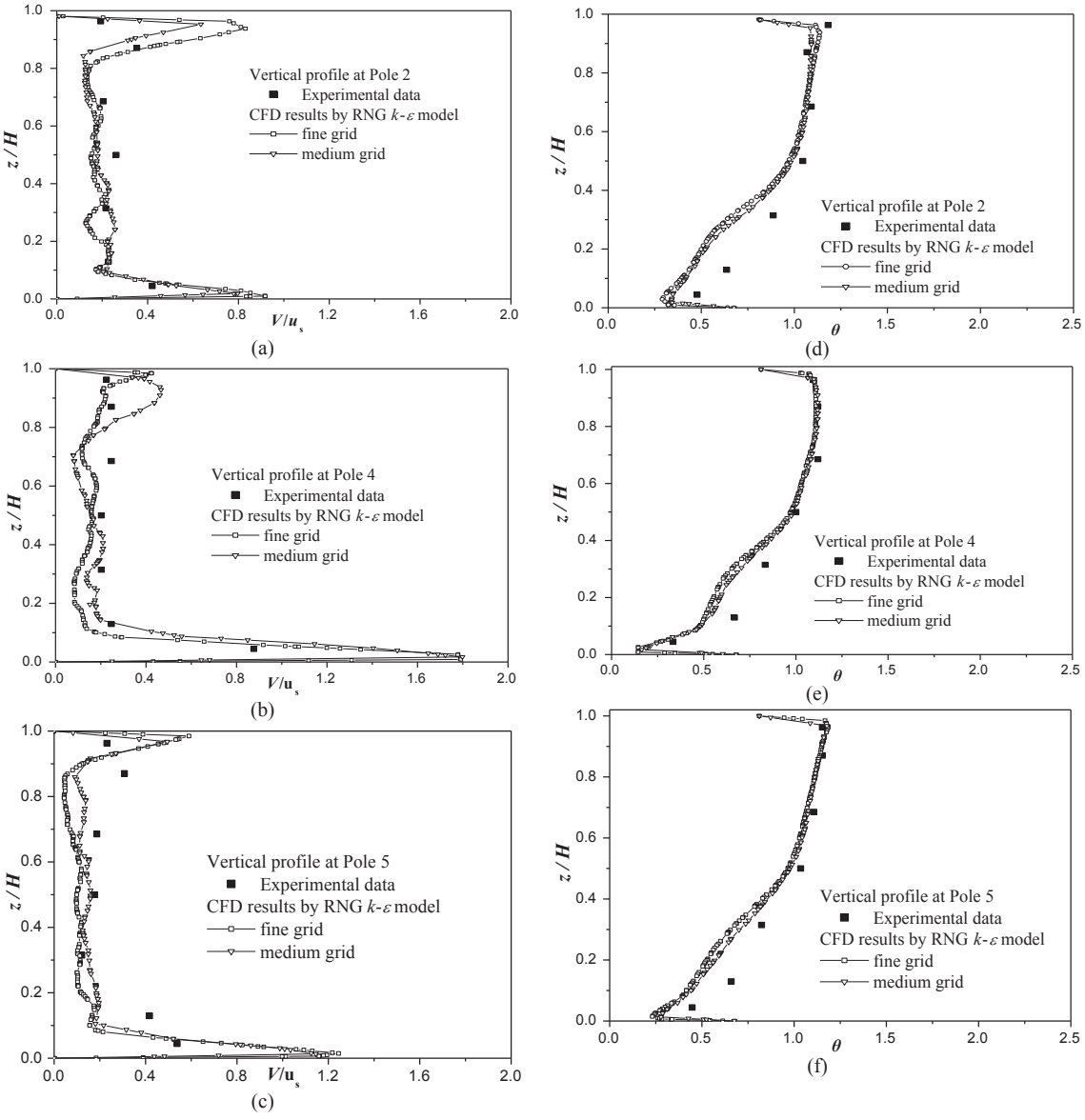

Fig. 4. Comparison of CFD results and experimental data: vertical profiles of velocity and temperature at (a) Pole 2, (b) Pole 4, (c) Pole 5.

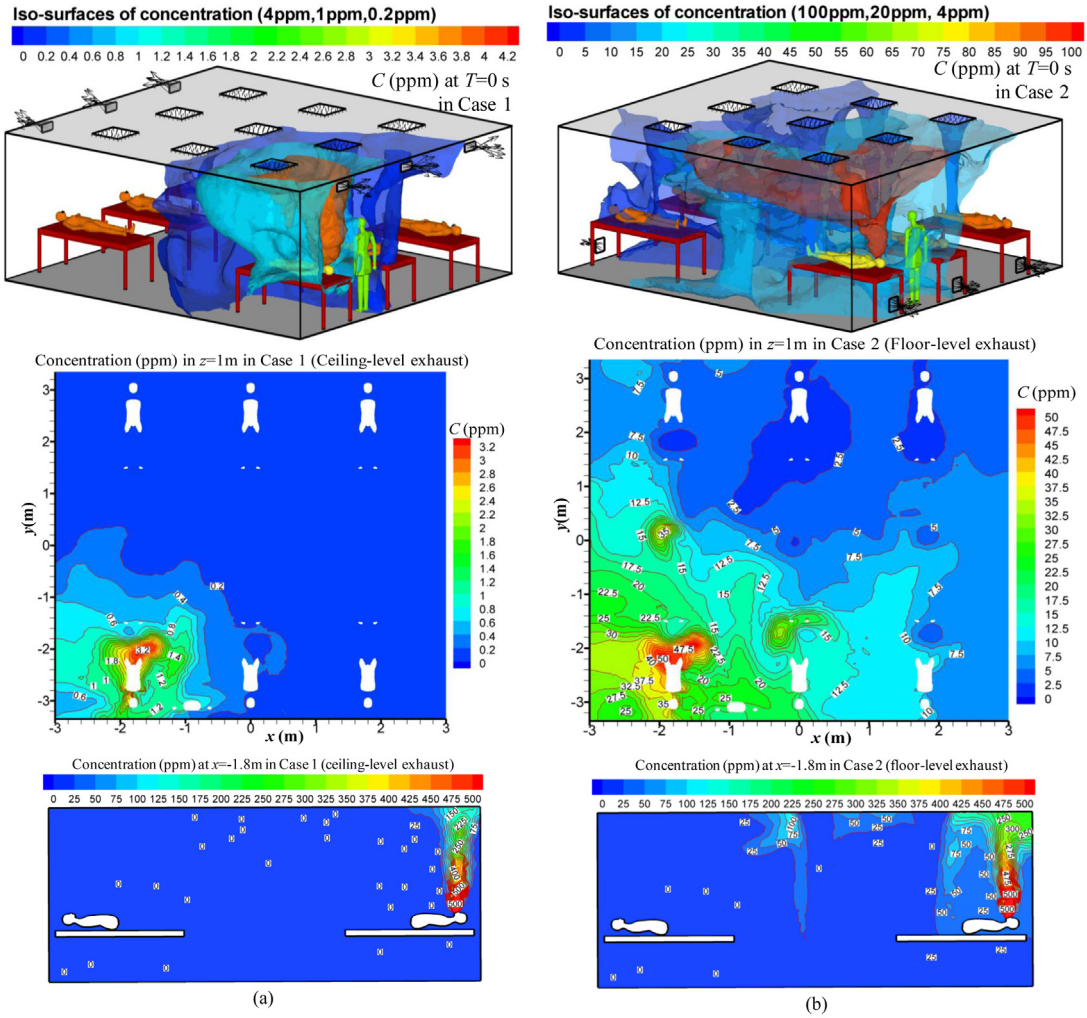

Fig. 5. Iso-surfaces of pollutant concentration (ppm) and concentration field in $z = 1$ m and $x = -1.8$ m in steady state ($t = 0$ s) of (a) Case 1, (b) Case 2. Temperature and flow vectors in $x = -1.8$ m in (c) Case 1 and (d) Case 2.

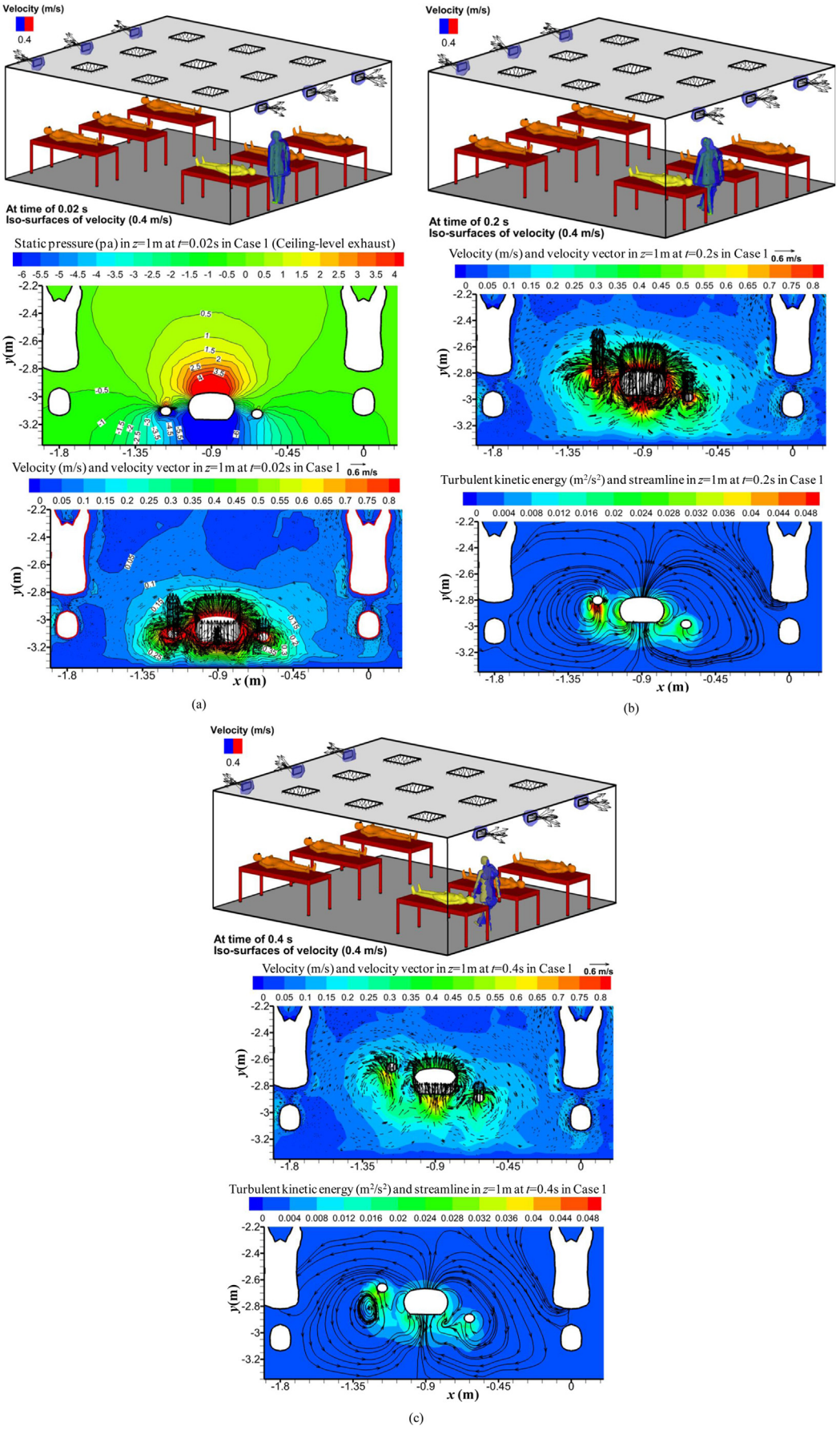

Fig. 6. Iso-surfaces of wind speed (0.4 m/s) and distribution of pressure and/or velocity vector and turbulent kinetic energy in $z = 1$ m in Case 1 at time of: (a) 0.02 s, (b) 0.2 s, (c) 0.4 s, (d) 0.7 s, (e) 3.6 s.

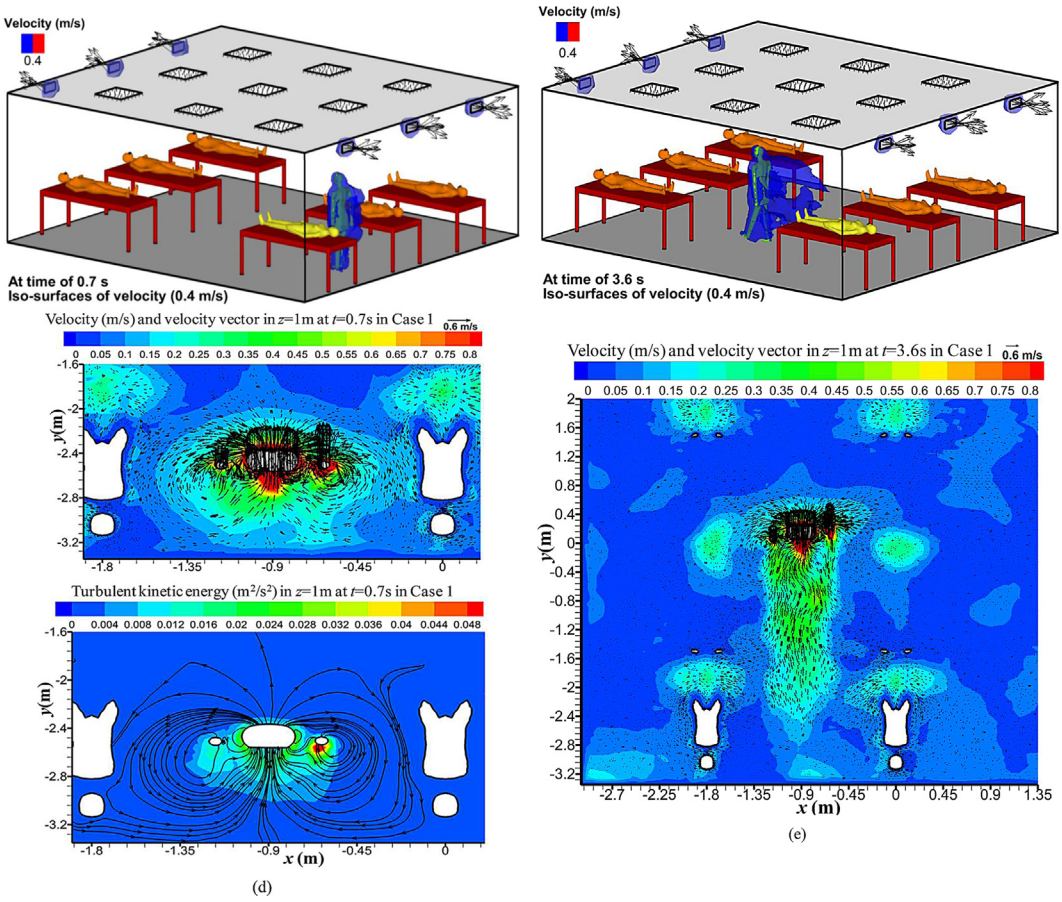

Fig. 6. (*continued*).

more flow disturbance. For example, Mazumda et al. [32] found that, if the body moves for 3 s and then stops, or it moves backwards and forwards in an one-bed isolation room with 4-ACH displacement ventilation system, the swing of gaseous concentration field will disappear in less than 60 s or in 90 s respectively.

As the first step, this paper only considers tracer gas simulation without moving backwards and forwards. CFD simulations of particles and droplets with different sizes will be included in the second paper. Five test cases were numerically investigated, as shown in Table 2. In Case 1 and Case 2, six ceiling-level or floor-level exhausts with the same air change rate of 12.9 ACH. In Case 3, an air change rate of 6 ACH with the ceiling-level exhausts is studied. The comparison of Case 1 and Case 3 is used to quantify the effect of the decreasing ventilation rate. In addition, the simplified HCW motion by moving rectangular objects with a constant velocity (0.89 m/s) is included in Case 4. Finally there is no heat flux from HCW surface in Cases 1–4. Thus in Case 5, the HCW surface heat flux of 57.5 Watt/m^2 is used.

3. Result and discussion

3.1. Assessment of CFD methodologies by experimental data

The reliability of CFD methodologies was first verified by the experimental data. measured by Yin et al. [19] within an inpatient ward (see Fig. 3) containing a bed, a TV set, a piece of medical equipment, a visitor, and a patient. Ventilation rate of 4 ACH (114 CFM) was obtained by air supplied from the diffuser located near the floor. Air was exhausted from the ward by the main exhaust and bathroom exhaust with the ventilation rate of 36 CFM and 78 CFM respectively. Fig. 3b shows locations of 8 poles where vertical profiles of velocity magnitude and static temperature were measured at the height of 0.12 m–2.6 m from the floor. The heat released from patient, caretaker, equipment and TV was 106 Watt, 110 Watt, 36 Watt, 24 Watt. More detailed information on experimental setups can be found in Yin et al. [19].

The medium and fine grid arrangements were utilized. For the former, about 0.38 million tetrahedral cells was used with the maximum grid size of 10 cm near wall surfaces and finer grid near heating surfaces. For the latter, about 1.8 million tetrahedral cells was produced with the maximum grid size of 5 cm near wall surfaces and finer grids near heating surfaces. The thermo-fluid boundary conditions in CFD simulations are shown in Table 3, which matched the experiment. The other CFD arrangements are the same with those introduced in Section 2. Fig. 4 shows vertical profiles of velocity and temperature at three example points of Pole 2, Pole 4 and Pole 5. The height, velocity, and temperature ($\theta = (T - T_s)/(T_e - T_s)$) were normalized with respect to the height of the inpatient ward ($H = 2.7$ m), supply air velocity ($u_s = 0.14$ m/s), temperature at inlet (T_s) and main exhaust (T_e). The temperature stratification is clearly found in CFD simulations. CFD results were in good agreement with the measured data. The medium grid does similarly good in CFD prediction as the find grid does. It depicts that present CFD arrangements using RNG k–ε model can predict indoor airflow generally well.

Though this paper does not carry out CFD validation for transient CFD simulations with moving objects because high-quality experimental data are rare [23–27]. Lee [43] verified that RNG k–

ε model [42] may successfully reproduce the transient turbulent flow over the square cylinder when high-order convection schemes are used. Zhang et al. [45] validated the CFD model in an airliner cabin under steady-state conditions. This steady-state model performed similarly for water flow in a small-scale experimental airliner cabin with transient conditions in Mazumdar et al. [28]. Thus the steady-state validation case in this inpatient ward could be used for test cases with HCW walking.

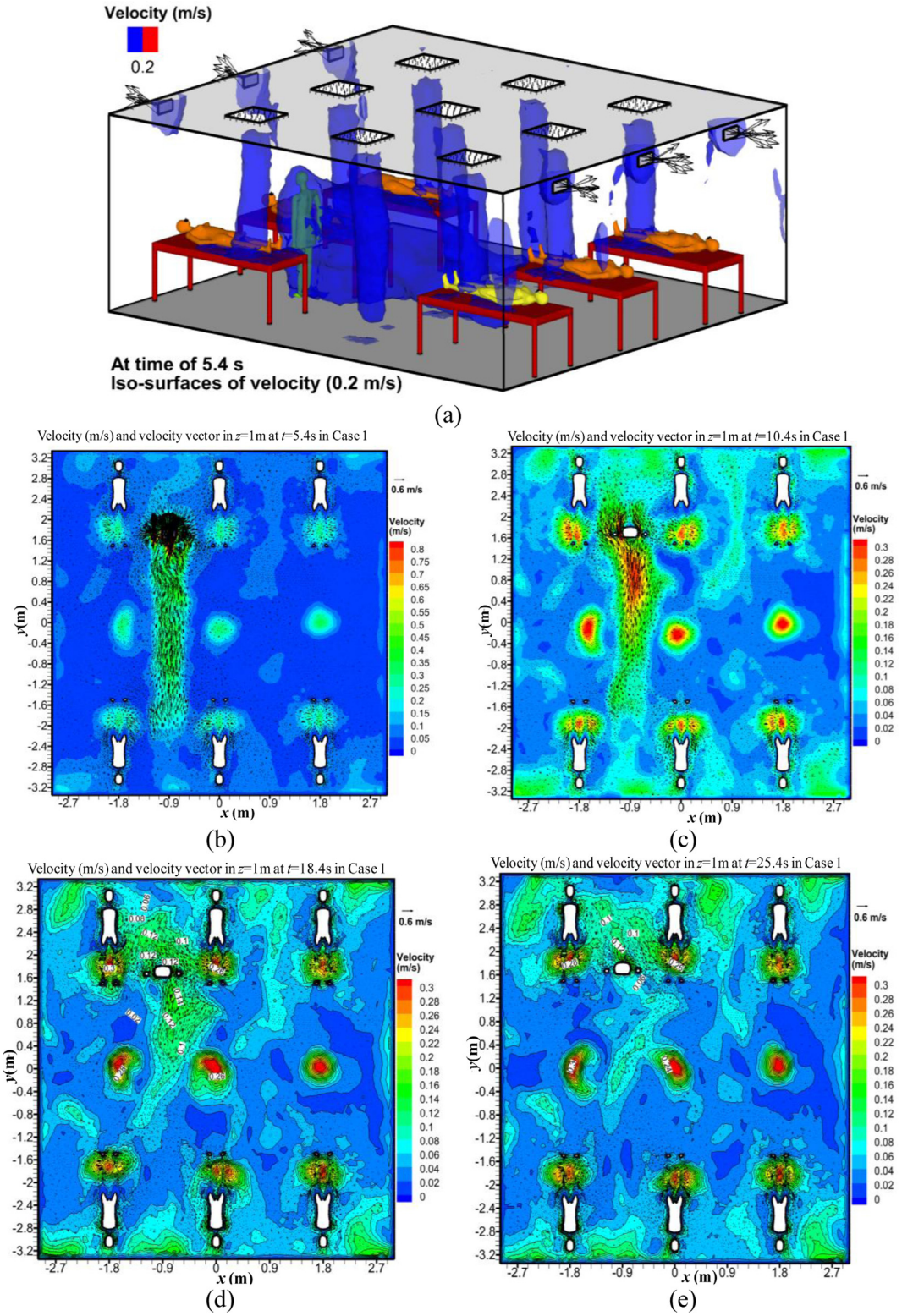

Fig. 7. (a) Iso-surfaces of wind speed (0.4 m/s and 0.2 m/s) in Case 1 at $t = 5.4$ s (the moment that HCW motion stops); Velocity vector in $z = 1$ m in Case 1 at time of (b) 5.4 s, (c) 10.4 s, (d) 18.4 s, (e) 25.4 s.

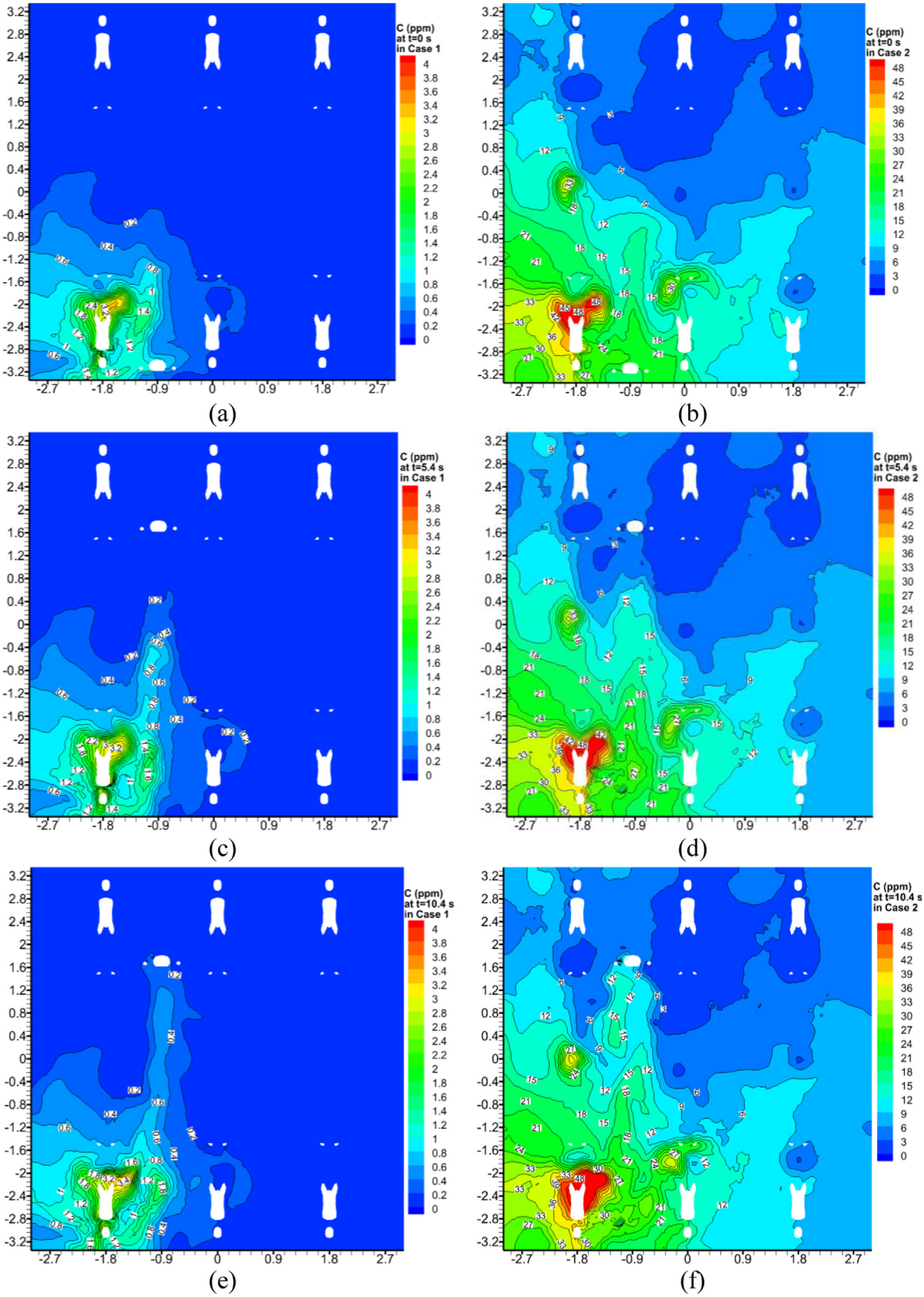

Fig. 8. Concentration (ppm) field in $z = 1$ m in Case 1 (left) and Case 2 (right) at time of (a and b) 0 s, (c and d) 5.4 s, (e and f) 10.4 s, (g and h) 18.4 s, (i and j) 25.4 s, (k) 35.4 s in Case 1 and (l) 55.4 s in Case 2.

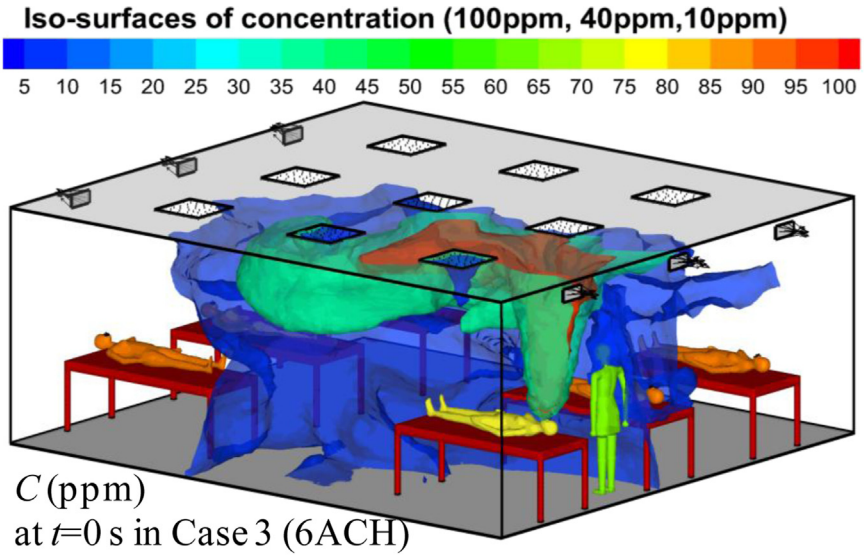

(a)

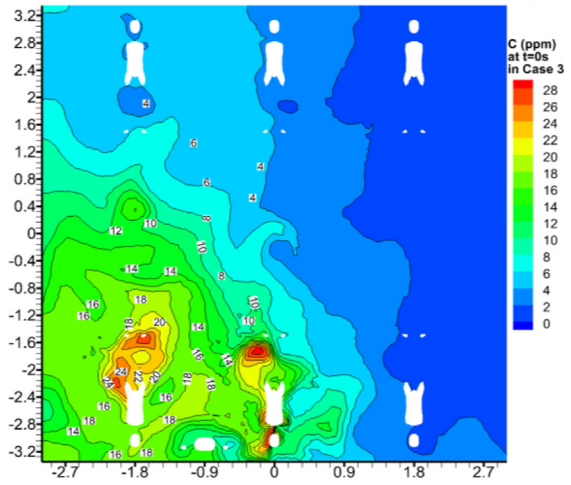

(b)

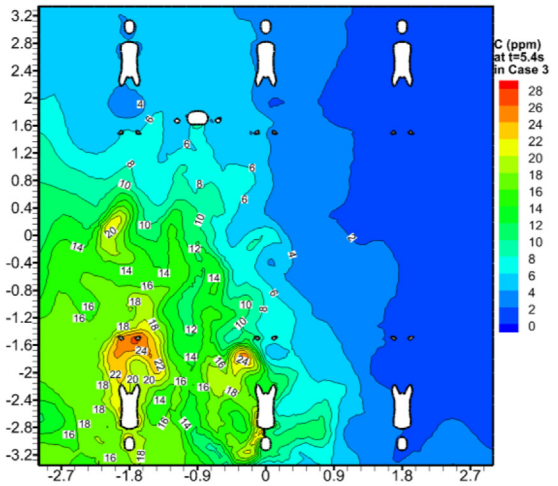

(c)

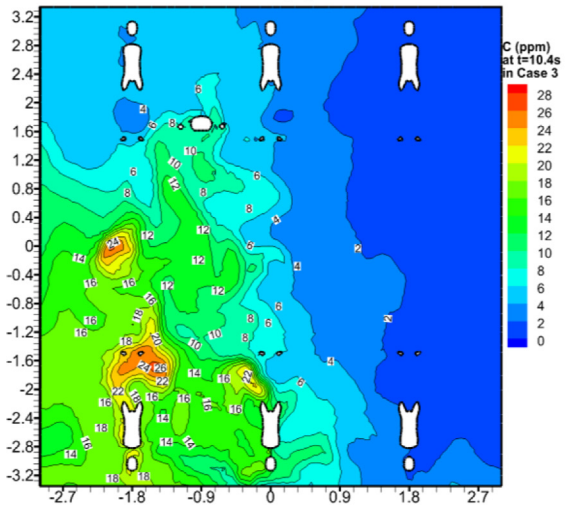

(d)

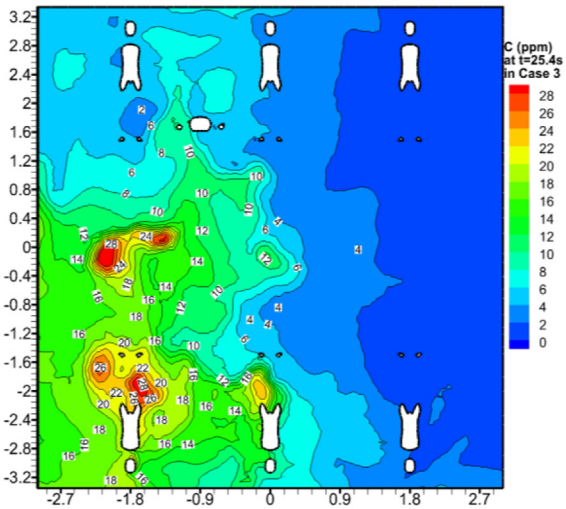

(e)

Fig. 9. (a) Iso-surfaces of concentration at time of 0 s in Case 3. Concentration field in $z = 1$ m in Case 3 at time of (b) 0 s, (c) 5.4 s, (d) 10.4 s, (e) 25.4 s, (f) 45.4 s, (g) 65.4 s.

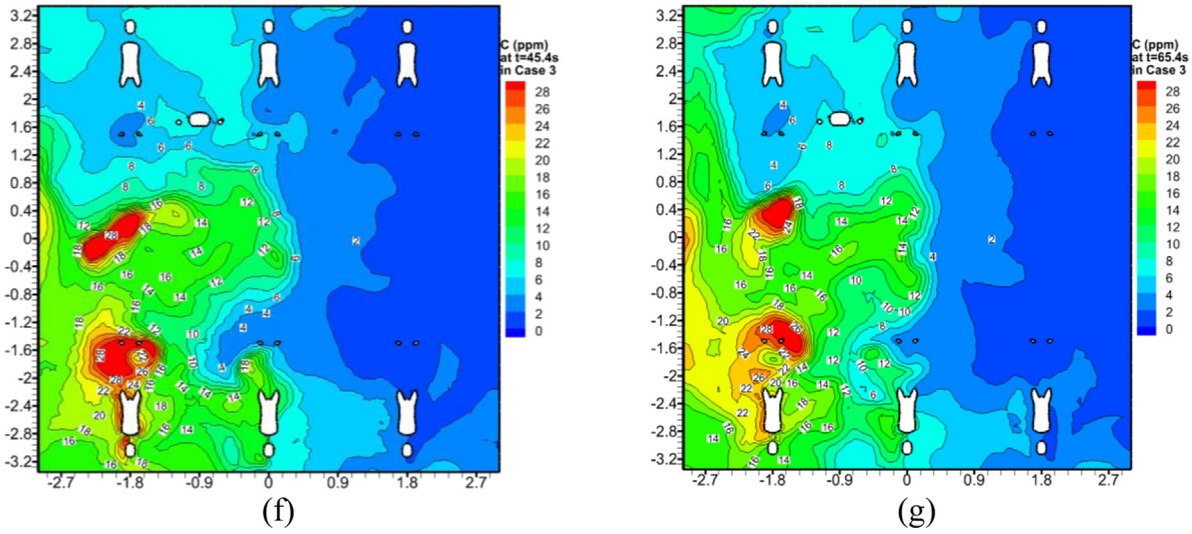

Fig. 9. (*continued*).

3.2. Effect of HCW motion under different exhaust designs

3.2.1. Steady-state flow and initial concentration field in Case 1 and Case 2

Fig. 5a and b shows iso-surfaces of tracer gas concentration as well as concentration field in $z = 1$ m and $x = -1.8$ m in Case 1 (12.9 ACH, ceiling-level) and Case 2 (12.9 ACH, floor-level) at steady state ($t = 0$ s). The concentration in Case 1 is much lower than that in Case 2. It confirms that the ceiling-level exhausts remove gaseous contaminants more efficiently than the floor-level exhausts. To explain this difference, Fig. 5c and d displays the flow vectors and temperature distribution in $x = -1.8$ m (the centre plane of source manikin) in Cases 1 and 2. The upward thermal plume above the lying patient model interacts with the main ventilation airflow. With the ceiling-level exhausts (Case 1, see Fig. 5c), this thermal plume above Patient 6 (source manikin) significantly enhances the upward flow induced by the ceiling-level exhausts and transports the exhaled contaminants to the ceiling level, part of which is removed out directly through the ceiling-level exhausts and the other joins the downward supply air stream. With the floor-level

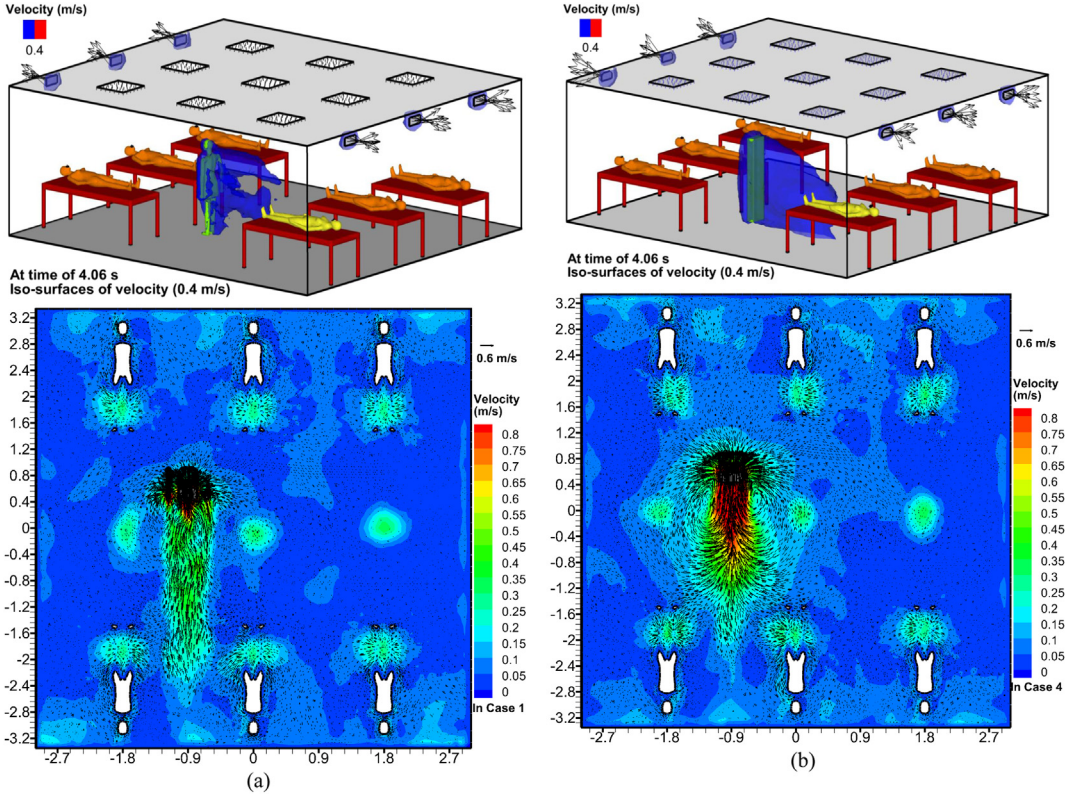

Fig. 10. Iso-surfaces of velocity at 0.4 m/s and velocity vector in $z = 1$ m at $t = 4.06$ s in: (a) Case 1 and (b) Case 4.

exhausts (Case 2, see Fig. 5d), the downward supply air streams in the middle of room fall vertically onto the floor and all gaseous contaminants leave the room through the floor-level exhausts below the beds. The interaction between the upward thermal plume and the two-side downward supply air stream induce a mixing airflow pattern above the lying manikins. Obviously the arrangement of floor-level exhausts is less efficient in removing gaseous contaminants. Similar findings have been reported by Qian and Li [18] that the ceiling-level exhausts are much more efficient than the floor-level exhausts in removing fine particles.

3.2.2. *Effect of HCW walking motion on flow and gaseous dispersion*

To show the flow disturbance induced by HCW walking, Fig. 6 displays iso-surfaces of wind speed (0.4 m/s), distribution of pressure, velocity vector and turbulent kinetic energy in $z = 1$ m in Case 1 at various time. HCW walking starts at $t = 0$ s. At time of 0.02 s, Fig. 6a shows that the velocity and pressure fields near the walking HCW model quickly change. There is a high pressure zone in front of the walking HCW, low pressure zone in the wake behind it, and a large velocity close to it. At time of 0.2 s (see Fig. 6b), there is more flow disturbance induced by the moving body and swinging arms/legs. The moving body displaces air in its front both forwardly and laterally, and its wake carries air forwardly. Meanwhile pressure difference (not shown here) induces air flowing from two lateral sides of the body to the wake behind the body, and also drives air flowing from the body front to the wake through the leakages between arms and the torso (or between two legs but not shown here). Moreover significant turbulence is produced near the walking HCW. Thus the realistic HCW walking does not simply

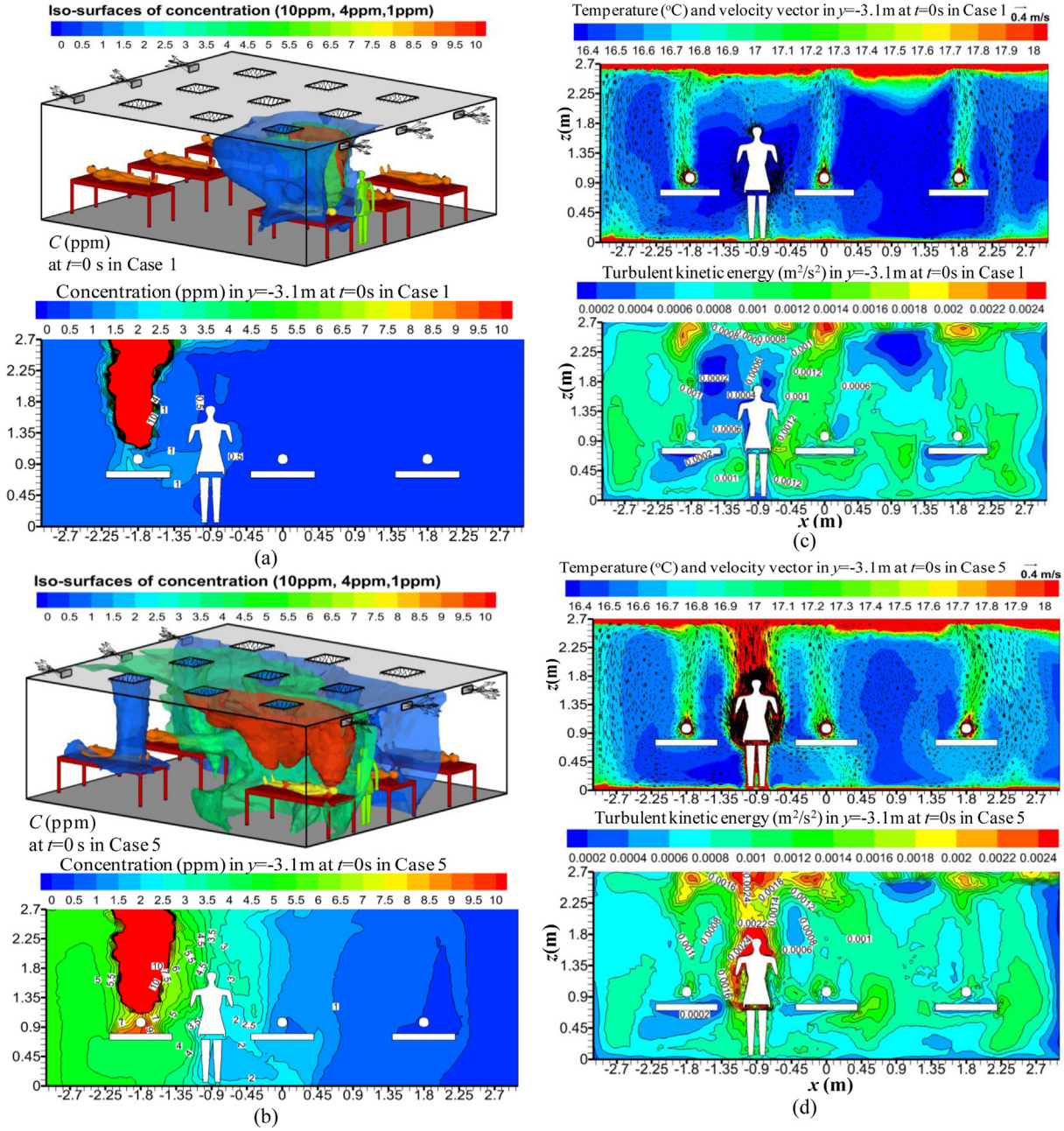

Fig. 11. Iso-surfaces of concentration and concentration in $y = -3.1$ m in (a) Case 1 and (b) Case 5. Temperature, velocity vector and turbulent kinetic energy in $y = -3.1$ in (c) Case 1 and (d) Case 5.

induce forward airborne transmission, but a complex mixing process. The temporal variation of walking speed is shown in Fig. 1b in which $t/T = 0.15$, 0.3,0.52 (or $t = 0.2$ s, 0.4 s, 0.7 s). At time of 0.4 s (see Fig. 6c), the disturbance of velocity and turbulence is weaker than that in Fig. 6b ($t = 0.2$ s) because the walking speed is relatively small at this moment. At time of 0.7 s (see Fig. 6d), the disturbance of velocity and turbulence near the walking body becomes large again because the walking speed is great at this moment. In Fig. 6a–d, the arms always swing with an opposite phase of legs. The walking speed and swinging motion of arms and legs vary cycle by cycle. At time of 3.6 s (Fig. 6e), the walking body is far from Patient 6 (i.e. source manikin). There is a forward flow in the wake which is about 2.5 m long.

To illustrate how the flow disturbance induced by HCW walking varies after the time of 5.4 s, Fig. 7a shows iso-surfaces of wind speed (0.4 m/s and 0.2 m/s) in Case 1 at $t = 5.4$ s. Then Fig. 7b–e displays velocity vector in $z = 1$ m in Case 1 at time of 5.4 s–25.4 s. At time of 5.4 s (see Fig. 7a and b), the wake with a forward flow is about 4.0 m long. The flow disturbance induced by human walking decreases after HCW walking stops (see Fig. 7b–e), but the residual flow disturbance still remains a little at time of 18.4 s and almost disappears at time of 25.4 s (i.e. 20 s after HCW walking stops).

3.2.3. How HCW walking affects airborne transmission of tracer gas

This subsection discusses how HCW walking affects gaseous contaminant transport. Fig. 8 displays concentration (ppm) field in $z = 1$ m in Case 1 (left, ceiling-level) and Case 2 (right, floor-level) at various time. For both cases, gaseous contaminant is transported from source manikin to the other side of the isolation room by the human-walking-induced wake formation and by the residual wake after HCW motion stops. Moreover the concentration field changes a little from 0 s to 5.4 s, and varies more from 5.4 s to 18.4 s after the HCW model stops walking. The above facts show that, it takes a while for airborne transmission to respond to the flow disturbance induced by human walking. In addition, the concentration field in Case 1 at time of 35.4 s (see Fig. 8k) is a little different from its initial state (see Fig. 8a, $t = 0$ s) because it has not returned to its initial state meanwhile HCW locations in the initial and final conditions are different; In Case 2 (see Fig. 8l), that at time of 55.4 s differs a little from its initial state (see Fig. 8b, $t = 0$ s) due to similar reason. It verifies that the ceiling-level exhausts is more effective to remove the human-motion-induced pollutant transport. Finally, Fig. 8 also confirms that the concentration in Case 1 is always much lower than that in Case 2no matter with or without HCW walking. Thus the ventilation design is still the first key parameter and much more significant than the effect of HCW motion.

3.3. Effect of air change rates and HCW geometry

Fig. 9a shows iso-surfaces of concentration at time of 0 s in Case 3 with air change rate of 6 ACH and the ceiling-level exhausts. Then Fig. 9b–g displays concentration field in $z = 1$ m at various time in Case 3. The comparison between Case 1 (Figs. 7 and 8, 12.9 ACH) and Case 3 (Fig. 9, 6 ACH) can show how the decreasing air change rate influences airborne transmission as HCW motion occurs.

In contrast to Case 1 (12.9 ACH, see Fig. 5a), Case 3 (6 ACH, see Fig. 9a) obviously attains much higher concentration at time of 0 s. As displayed in Fig. 9, the human-walking-induced flow disturbance from 0 s to 5.4 s indeed produces gaseous contaminant transport from source manikin to the other side of the isolation room, but its residual flow produces more airborne spread from 5.4 s to 25.4 s after the HCW stops walking. Although the concentration field tends to return its initial state after time of 25.4 s, but there is still a little higher concentration near the HCW model at time of 45.4 s and 65.4 s (see Fig. 9f–g) than at time of 0 s (see Fig. 9a). It verifies that, in contrast to Fig. 8k with 12.9 ACH, it takes more than 60 s in Case 3 (6 ACH) to remove or dilute pollutants near the stopped HCW model. In addition, the concentration in Case 1 (see Figs. 7 and 8, 12.9 ACH) is always much lower than that in Case 3 (see Figs. 9, 6 ACH) no matter whether HCW motion occurs. Therefore air change rate is another much more significant parameter than HCW walking in affecting airborne transmission.

Then in comparison to realistic HCW motion in Case 1 (Body A), the effect of simplified forward motion by a rectangular block (Body B) is investigated in Case 4with the same ceiling-level exhausts and air change rates (12.9 ACH). To the difference of flow disturbance induced by HCW geometries, Fig. 10 displays iso-surfaces of velocity at 0.4 m/s and flow field in $z = 1$ m at time of 4.06 s in Case 1 and Case 4. The realistic HCW motion (see Fig. 10a) obviously induces less flow disturbance than the simplified one (see Fig. 10b). The reason is that, the realistic Body A is a blunt geometry which has leakage between arms and the torso and between two legs. Body B has sharp-edged boundaries without such leakage, and it subsequently produces a stronger flow disturbance than Body A, enhancing the displacement flow in front of the body and strengthening the wake formation behind it.

3.4. Effect of surface heat fluxes of HCW model

In Case 1 to Case 4, it assumes that HCW model only stay near the source manikin for a short moment (much less than 5 min) and there is no heat flux from HCW surface. This subsection considers another situation that HCW model has stayed there for sufficiently long time (for example more than 10 min), thus the surface heat flux (57.5 Watt/m^2) of HCW model is taken into account in Case 5.

Fig. 11a and b displays 3D iso-surfaces of concentration and concentration field in $y = -3.1$ m of Case 1 and Case 5 at their initial conditions ($t = 0$ s). With the HCW surface heat flux (Case 5, see Fig. 11b), gaseous contaminants released from the source manikin tend to spread more to the surrounding than Case 1. To illustrate the mechanisms, Fig. 11c and d shows temperature, velocity vector and turbulent kinetic energy in $y = -3.1$ in Case 1 and Case 5. Obviously the thermal plume and turbulence surrounding and above the heated standing HCW model are stronger (Case 5, see Fig. 11d) than Case 1 (see Fig. 11c). The stronger thermal plume and turbulence induced by the heated HCW model slightly enhance airborne transmission.

Finally Fig. 12 shows concentration field in $z = 1$ m in Case 5 at various time. There is similar finding that, not only the flow disturbance induced by HCW motion (i.e. from 0 s to 5.4 s) but also its residual flow disturbance after HCW motion stops (i.e. from 5.4 s to 25.4 s) produces airborne transmission from the source manikin to the other side of the room. At time of 35.4 s (see Fig. 12f), the concentration field still differs a little from the initial state (see Fig. 12a).

4. Conclusions

This paper integrates the dynamic mesh technique with unsteady CFD simulations using RNG k–ε model to study how HCW motion affects the flow and airborne transmission in a six-bed isolation room. Tracer gas is first used to simulate respiratory droplet nuclei released from the mouth of the source thermal manikin. Ventilation systems consist of six ceiling-level or floor-level exhausts on vertical walls, nine downward supplies on the ceiling. HCW model first walks for 5.4 s from the initial location near the source manikin to the other side of the isolation room, then it stops there for 60 s. The HCW walking indeed produces the flow disturbance and enhances airborne transmission from the source manikin to the other side, but the exhaust locations and air

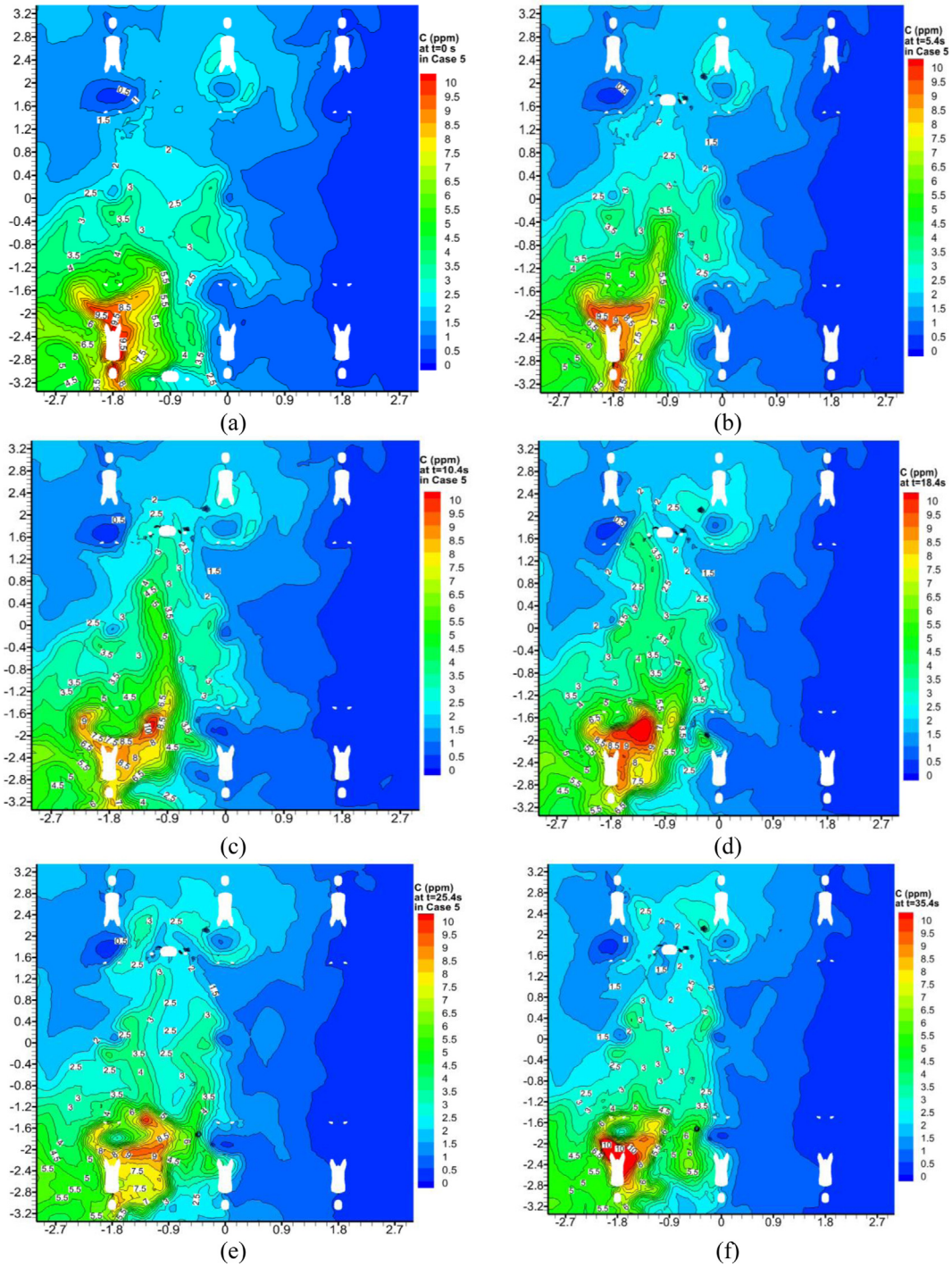

Fig. 12. Concentration field in $z = 1$ m in Case 5 at various time of (a) 0 s, (b) 5.4 s, (c) 10.4 s, (d) 18.4 s, (e) 25.4 s, (f) 35.4 s.

change rates are found more important than HCW walking. No matter with or without HCW motion, the ceiling-level exhausts with the air change rate of 12.9 ACH attain much lower concentration in this isolation room than the floor-level exhausts (12.9 ACH); With the same ceiling-level exhausts, a smaller air change rate (6 ACH) always experiences much higher concentration than a greater one (12.9 ACH).

During HCW motion occurs, the flow quantities including pressure, velocity and turbulence near and behind human body are all easily influenced by HCW motion. During the duration of HCW motion (5.4 s), tracer gas spreads a little from the source manikin to the other side, however after HCW walking stops the residual wake continues to induce more gaseous spread. It takes more than 30 s–60 s for the concentration field to approximately return to its initial state after HCW walking stops. The motion of HCW walking produces a complex mixing process. For realistic human walking with swinging legs and arms, the moving body displaces air parcels in front of the body forwardly and laterally, meanwhile a large pressure difference drives air from two lateral sides of HCW to the wake and from the body front backward to the wake through gaps

between arms and legs. Significant turbulence is produced near HCW body. The simplified motion of rectangular block generates unrealistic stronger flow disturbance than realistic HCW walking.

It should be noted that this paper only takes limited conditions into account. Although further investigations are still required to consider the dispersion and depositions of particles and droplets, to vary the speed of walking speed, to simulate other exhaling activities, such as talking, sneezing, and coughing, this paper provides meaningful findings for understanding how HCW walking influences airborne transmission in a multi-bed isolation room.

Acknowledgement

This study was financially supported by the National Natural Science Foundation of China (No. 51278440 and No. 51108102) and the Fundamental Research Funds for the Central Universities of Sun Yat-sen University (No. 2013390003165002). Dr Yonggao Yin and Dr Hua Qian in Southeast University P. R. China who provided kind help, the two anonymous reviewers who provided constructive suggestions and comments as well as the special concern from the Control of Infectious Diseases (RFCID) and the Hospital Authority (HA) of Hong Kong are all gratefully acknowledged.

References

[1] Gao N, Niu J, Perino M, Heiselberg P. The airborne transmission of infection between flats in high-rise residential buildings: tracer gas simulation. Build Environ 2008;43:1805–17.
[2] Li Y, Huang X, Yu ITS, Wong TW, Qian H. Role of air distribution in SARS transmission during the largest nosocomial outbreak in Hong Kong. Indoor Air 2004;15:83–95.
[3] Li Y, Leung GM, Tang JW, Yang X, Chao CYH, Lin JZ, et al. Role of ventilation in airborne transmission of infectious contaminants in the built environment - a multidisciplinary systematic review. Indoor Air 2007;17:2–18.
[4] Tang JW, Li Y, Eames I, Chan PKS, Ridgway GL. Factors involved in the aerosol transmission of infection and control of ventilation in healthcare premises. J Hosp Infect 2006;64:100–14.
[5] Beggs CB, Kerr KG, Noakes CJ, Hathway EJ, Sleigh PA. The ventilation of multiple-bed hospital wards: review and analysis. Am J Infect Control 2008;36:250–9.
[6] Zhao B, Zhan Y, Li X, Yang X, Huang D. Comparison of indoor aerosol particle concentration and deposition in different ventilated rooms by numerical method. Build Environ 2004;39:1–8.
[7] Chen C, Zhao B, Yang X, Li Y. Role of two-way airflow owing to temperature difference in SARS transmission – revisiting the largest nosocomial SARS outbreak in Hong Kong. J R Soc Interface 2011;8:699–710.
[8] Chen C, Zhao B. Some questions on dispersion of human exhaled droplets in ventilation room: answers from numerical investigation. Indoor Air 2010;20(2):95–111.
[9] Lai AC. Particle deposition indoors: a review. Indoor Air 2002;12:211–4.
[10] Nazaroff WW. Indoor particle dynamics. Indoor Air 2004;14:175–83.
[11] Zhao B, Zhang Z, Li X. Numerical study of the transport of droplets or particles generated by respiratory system indoors. Build Environ 2005;40:1032–9.
[12] Shen C, Gao N, Wang T. CFD study on the transmission of indoor pollutants under personalized ventilation. BuildEnviron 2013;63:69–78.
[13] Saravia SA, Raynor PC, Streifel AJ. A performance assessment of airborne infection isolation rooms. Am J Infect Control 2007;35:324–31.
[14] Qian H, Li Y, Nielsen PV, Hyldgaard CE, Wong TW, Chwang ATY. Dispersion of exhaled droplet nuclei in a two-bed hospital ward with three different ventilation systems. Indoor Air 2006;16:111–28.
[15] Tung YC, Hu SC, Tsai TI, Chang IL. An experimental study on ventilation efficiency of isolation room. Build Environ 2009;44:271–9.
[16] Yin Y, Gupta JK, Zhang X, Liu J, Chen Q. Distributions of contaminant exhaled out by a patient with different postures and exhaling modes in a single-bed inpatient room. Build Environ 2011;46:75–81.
[17] Qian H, Li Y, Nielsen PV, Hyldgaard CE. Dispersion of exhalation pollutants in a two-bed hospital ward with a downward ventilation system. Build Environ 2008;43:344–54.
[18] Qian H, Li Y. Removal of exhaled particles by ventilation and deposition in a multibed airborne infection isolation room. Indoor Air 2010;20:284–97.
[19] Yin Y, Xu W, Gupta JK, Guity A, Marmion P, Manning A, et al. Experimental study on displacement and mixing ventilation systems for a patient ward. HVAC&R Res 2009;15:1175–91.
[20] Brohus H, Nielsen PV. Personal exposure in displacement ventilated rooms. Indoor Air 1996;6:157–67.
[21] Tang JW, Noakes CJ, Nielsen PV, Eames I, Nicolle A, Li Y, et al. Observing and quantifying airflows in the infection control of aerosol- and airborne-transmitted diseases: an overview of approaches. J Hosp Infect 2011;77(3):213–22.
[22] Chen Q. Ventilation performance prediction for buildings: a method overview and recent applications. Build Environ 2009;44:848–58.
[23] Mattsson M. On the efficiency of displacement ventilation – with particular reference to the influence of human activity [PhD thesis]. Gavle, Sweden: Royal Institute of Technology; 1999.
[24] Matsumoto H, Ohba Y. The influence of a moving object on air distribution in displacement ventilated rooms. J Asian Archit Build 2004;3:71–5.
[25] Bjørn E, Nielsen PV. Dispersal of exhaled air and personal exposure in displacement ventilated rooms. Indoor Air 2002;12:147–64.
[26] Liu W, Mazumdar S, Zhang Z, Poussou SB, Liu JJ, Lin CH, et al. State-of-the-art methods for studying air distributions in commercial airliner cabins. Build Environ 2012;47:5–12.
[27] Poussou SB, Mazumdar S, Plesniak MW, Sojka PE, Chen QY. Flow and contaminant transport in an airliner cabin induced by a moving body: model experiments and CFD predictions. Atmos Environ 2010;44:2830–9.
[28] Mazumdar S, Poussou SB, Lin CH, Isukapalli SS, Plesniak MW, Chen QY. Impact of scaling and body movement on contaminant transport in airliner cabins. Atmos Environ 2011;45:6019–28.
[29] Choi JI, Edwards JR. Large eddy simulation and zonal modeling of human induced contaminant transport. Indoor Air 2008;18:233–49.
[30] Choi JI, Edwards JR. Large-eddy simulation of human-induced contaminant transport in room compartments. Indoor Air 2012;22(1):77–87.
[31] Shih YC, Chiu CC, Wang O. Dynamic airflow simulation within an isolation room. Build Environ 2007;42:3194–209.
[32] Mazumdar S, Yin Y, Guity A, Marmion P, Gulick B, Chen Q. Impact of moving objects on contaminant concentration distributions in an inpatient room with displacement ventilation. HVAC&R Res 2010;16:545–64.
[33] Wang J, Chow TT. Numerical investigation of influence of human walking on dispersion and deposition of expiratory droplets in air-borne infection isolation room. Build Environ 2011;46:1993–2002.
[34] Edge BA, Paterson EG, Settles GS. Computational study of the wake and contaminant transport of a walking human. J Fluid Eng 2005;127:967–77.
[35] Gao NP, Niu JL. CFD study of the thermal environment around a human body: a review. Indoor Built Environ 2005;14:5–16.
[36] Tung Y, Shih Y, Hu S. Numerical study on the dispersion of gaseous contaminants from an isolation room in the case of door opening. Appl Therm Eng 2009;29:1544–51.
[37] Tang JW, Eames I, Li Y, Taha YA, Wilson P, Bellingan G, et al. Door-opening motion can potentially lead to a transient breakdown in negative-pressure isolation conditions: the importance of vorticity and buoyancy airflows. J R Soc Interface 2005;61:283–96.
[38] Eames I, Shoaib D, Klettner CA, Taban V. Movement of gaseous contaminants in a hospital isolation room. J R Soc Interface 2009;6:S757–66.
[39] Ronan B, Branislav U, Daniel T. Versatile walk engine. CH-1015 Lausanne, Switzerland: Virtual Reality Laboratory, I&C, EPFL; 2004.
[40] Ainsworth BE, Haskell WL, Whitt MC, Irwin ML, Swartz AM, Strath SJ, et al. Compendium of physical activities: an update of activity codes and MET intensities. Med Sci Sport Exer 2000;32(9):S498–516.
[41] FLUENT V6.3. User's manual.http://www.fluent.com; 2006.
[42] Ferziger JH, Peric M. Computational methods for fluid dynamics. Berlin, New York: Springer; 2002.
[43] Lee S. Unsteady aerodynamic force prediction on a square cylinder using $k-\varepsilon$ turbulence models. J Wind Eng Ind Aerodyn 1997;67–68:79–90.
[44] Zhang Z, Zhang W, Zhai Z, Chen Q. Evaluation of various turbulence models in predicting airflow and turbulence in enclosed environments by CFD: Part- 2: comparison with experimental data from literature. HVAC&R Res 2007;13(6):871–86.
[45] Zhang Z, Chen X, Mazumdar S, Zhang TF, Chen Q. Experimental and numerical investigation of airflow and contaminant transport in an airliner cabin mockup. Build Environ 2009;44:85–94.
[46] Brohus H. Personal exposure to contaminant sources in ventilated rooms [PhD thesis]. Aalborg, Denmark: Aalborg University; 1997.
[47] Gupta JK, Lin CH, Chen Q. Flow dynamics and characterization of a cough. Indoor Air 2009;19:517–25.
[48] Gupta JK, Lin CH, Chen Q. Characterizing exhaled airflow from breathing and talking. Indoor Air 2010;20:31–9.
[49] Zhao B, Wu J. Numerical investigation of particle diffusion in a clean room. Indoor Built Environ 2005;14:469–79.